Analytical Methods

ROYAL SOCIETY OF CHEMISTRY

PAPER

View Article Online
View Journal

Cite this: DOI: 10.1039/d1ay00320h

Fast detection of *E. coli* with a novel fluorescent biosensor based on a FRET system between UCNPs and GO@Fe_3O_4 in urine specimens†

Yuan Yao,[a] Guoming Xie,[b] Xin Zhang,[a] Jinshan Yuan,[a] Yulei Hou[a] and Hui Chen *[a]

Received 24th February 2021
Accepted 2nd April 2021

DOI: 10.1039/d1ay00320h

rsc.li/methods

Biosensors based on nanomaterials are becoming a research hotspot for the rapid detection of pathogenic bacteria. Herein, a "turn-on" fluorescent biosensor based on a FRET system was constructed for the fast detection of a representative pathogenic microorganism, namely, *E. coli*, which causes most urinary tract infections. This biosensor was constructed by utilizing synthesized UCNPs as fluorescent donors with stable luminescence performance in complex biological samples and GO@Fe_3O_4 as a receptor with both excellent adsorption ability and fluorescence quenching ability. A specific ssDNA selected as an aptamer which could recognize *E. coli* was immobilized on the UCNPs to form UCNP-Apt nanoprobes. The nanoprobes were adsorbed on the surface of GO@Fe_3O_4 through the π-stacking interactions between aptamers and GO. In the presence of *E. coli*, UCNP-Apt nanoprobes detached from GO@Fe_3O_4 due to the specific recognition of aptamers and bacteria, resulting in obvious fluorescence recovery, and the concentration of bacteria was positively correlated with the intensity of the fluorescence signal; such a "turn-on" signal output mode ensures excellent precision. In addition, the easy magnetic separation of GO@Fe_3O_4 simplifies the operation process, helping the sensor detect bacteria in 30 minutes with a linear range from 10^3 to 10^7 CFU mL^{-1} and a limit of detection of 467 CFU mL^{-1}. Moreover, recovery test results also showed that the sensor has clinical application potential for the rapid detection of pathogenic microorganisms in complex biological samples.

Introduction

Bacterial urinary tract infections (UTIs) are a common infectious disease, and 80% of UTIs are caused by *Escherichia coli* (*E. coli*).[1] The treatment of bacterial infections mainly depends on the assistance of antibiotics. To avoid antimicrobial resistance caused by drug abuse, sufficient laboratory evidence should be provided before the application of antibiotics, such as microorganism identification and drug sensitivity tests. As the gold standard, bacterial culture requires an enrichment step to increase the number of bacteria to reach the minimum detection level, and the entire process of culture and identification takes at least 48 h, which might result in the delay of treatment. Shortening the detection time can help clinicians formulate appropriate treatment plans in a timely manner, which will lead to better therapeutic effects and lower costs. The quantitative detection of bacteria can be achieved by the polymerase chain reaction (PCR) with high sensitivity, but they are susceptible to contamination, which produces false positive signals.[2–4] Mass spectrometry is another attractive detection method that has been clinically accepted;[5–8] however, the high costs and complicated operative procedure limit its application in resource-limited areas. Therefore, a simple and rapid method for the diagnosis of pathogenic bacteria is urgently needed.

Recently, nanomaterial-based biosensors for pathogenic bacteria detection have become a research hotspot in point-of-care tests.[9–11] Federico Schaumburg *et al.* designed an isotachophoretic microfluidic paper-based analytical device to complete the detection of *E. coli* in 90 min.[12] Sanjay Singh *et al.* reported a vancomycin-coated impedance sensor for discriminating Gram-positive and Gram-negative bacteria, and the limit of detection was 10^2 CFU mL^{-1} with a linear dynamic range of 10^2 to 10^7 CFU mL^{-1}.[13] In our previous research, a new type of enzyme-free electrochemical biosensor was constructed based on highly catalytic Cu–ZrMOF and conductive Super P, achieving the rapid detection of *Pseudomonas aeruginosa* within 120 min.[14] These studies indicate that biosensors based on nanomaterials have high application potential for the rapid detection of pathogens.

[a]*Clinical Laboratories, The First Affiliated Hospital of Chongqing Medical University, Chongqing, 400016, P. R. China. E-mail: huichen@cqmu.edu.cn*

[b]*Key Laboratory of Laboratory Medical Diagnostics, Chinese Ministry of Education, Department of Laboratory Medicine, Chongqing Medical University, Chongqing, 400016, P. R. China. E-mail: guomingxie@cqmu.edu.cn*

† Electronic supplementary information (ESI) available. See DOI: 10.1039/d1ay00320h

Fluorescent biosensors have usually been used for the detection of targets due to their low cost, common detection equipment and simple operation.[15–18] However, traditional organic fluorescent dyes have the characteristics of a short fluorescence lifetime, unstable optical properties, and severe background signals, which limit their application in the detection of complex biological samples.[19–22] Upconversion nanoparticles (UCNPs) are a new type of nanoluminescence material that converts near-infrared light into shortwave radiation (anti-Stokes law light, also known as upconversion light) through a multiphoton absorption mechanism, and their emission wavelength can be adjusted by doping different rare earth ions at various ratios.[23] Compared with traditional organic fluorescent dyes, UCNPs have stable optical properties and are less prone to photobleaching.[24–27] When excited by near infrared light, the excitation light is not affected by background absorption and autofluorescence during the detection of complex biological samples. Therefore, it has many applications in the detection of targets.[28–32]

Graphene oxide (GO) is a two-dimensional layered material that can not only strongly adsorb single-stranded DNA (ssDNA) through π-stacking interactions but also efficiently load more biomolecules or nanomaterials because of its large specific area.[33] Meanwhile, it has a wide range of applications in fluorescent sensors due to its fluorescence quenching ability.[34–37] However, the detection performance of the biosensor in sample analysis will be affected by its poor water solubility and shading effect. In our previous work,[38] we found that the GO@Fe_3O_4 nanocomposite has better water solubility than GO alone. Moreover, the nanocomposite retains excellent fluorescence quenching performance and a large specific area with many binding sites to load biomolecules or nanoprobes, and it is easily separated with a magnet due to containing Fe_3O_4.

Herein, a novel fluorescent biosensor was constructed based on fluorescence resonance energy transfer (FRET) between UCNPs and GO@Fe_3O_4. The UCNP nanoprobes which could recognize *E. coli* were adsorbed on the surface of GO@Fe_3O_4 to form a FRET system, leading to the fluorescence quenching of UCNPs at 475 nm. After incubation with target bacteria, the upconversion fluorescence at 475 nm was recovered and the concentration of bacteria was positively correlated with the intensity of the fluorescence signal. The assay principle is depicted in Scheme 1.

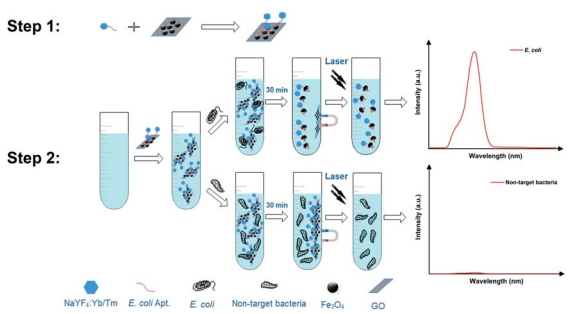

Scheme 1 Schematic of the fluorescence biosensor for *E. coli* detection. Step 1: the construction process of the biosensor; step 2: the detection process of *E. coli*.

Experimental section

Materials and instruments

All commercial chemicals were of analytical grade and used without further purification unless stated otherwise. *E. coli* (ATCC 25923) was obtained from the American Type Culture Collection (ATCC, USA). *Staphylococcus aureus* (*S. aureus*), *Acinetobacter baumannii* (*A. baumannii*), and *P. aeruginosa* were gifted by the First Affiliated Hospital of Chongqing Medical University. Rare earth chlorides $YCl_3 \cdot 6H_2O$, $YbCl_3 \cdot 6H_2O$, $TmCl_3 \cdot 6H_2O$, NaOH and NH_4F were purchased from Aladdin Reagent, Ltd. (Shanghai, China). Poly(acrylic acid sodium salt), 1-ethyl-3-(3-dimethylaminopropyl)carbodiimide hydrochloride (EDC), oleic acid (90%), and 1-octadecene (90%) were purchased from Sigma Aldrich (St. Louis, USA). mPEG-NH_2 (methoxypolyethylene glycol ammonia) was purchased from Macklin (Shanghai, China). Hydroxysulfosuccinimide sodium salt (Sulfo-NHS) and HEPES (1 M, pH 7.5–8.0) were purchased from Sangon Biotechnology Co., Ltd. (Shanghai, China). DNA oligonucleotides were synthesized, modified and HPLC-purified at Sangon Biotechnology Co., Ltd. (Shanghai, China). The sequences and modification of DNA strands are shown in the ESI (Table S2†). GO@Fe_3O_4 was purchased from XFNANO (Nanjing, China). Ultra-pure water (Milli-Q 18.2 MΩ, Millipore System Inc.) was used to prepare all aqueous solutions. Transmission electron microscopy (TEM) (H600, Hitachi, Japan) was used to investigate the size, morphology, and microstructure of the as-prepared nanoparticles. Fourier transform infrared (FT-IR) spectroscopy was performed on a Fourier transform infrared spectrophotometer (Thermo Fisher, USA). The zeta potential was measured using a Nano-ZEN3600 Zetasizer system (Malvern, UK) at 25 °C. UV-Vis-NIR spectra were recorded with a Shimadzu UV-2550 spectrophotometer (Shimadzu Co., Kyoto, Japan). Fluorescence measurements were carried out on a Cary Eclipse fluorescence spectrophotometer (Agilent Technologies, USA) using a 2 W 980 nm CW laser (Hi-tech Optoelectronics Co., Ltd., Beijing, China) as the excitation source.

Synthesis and surface modification of UCNPs

UCNPs were synthesized according to the hydrothermal method with some modifications.[39] Briefly, 482.30 mg of $YCl_3 \cdot 6H_2O$, 155.00 mg of $YbCl_3 \cdot 6H_2O$, and 2.75 mg of $TmCl_3 \cdot 6H_2O$ were added to a flask containing 18 mL of oleic acid and 30 mL of 1-octadecene, and heated to 160 °C for 90 min in an argon flow. After the solution was cooled to room temperature, 10 mL of methanol containing 296.30 mg of NH_4F and 200.00 mg of NaOH were added to the flask and stirred at 50 °C for 30 min. Then, the mixed solution was heated to 100 °C and held for another 30 min to remove residual methanol. Subsequently, the solution was heated to 300 °C for 120 min and then cooled to room temperature. Finally, the mixture was washed three times with ethanol and dispersed in cyclohexane.

The as-synthesized UCNPs were transferred into the aqueous phase through an acid-induced ligand removal process. The UCNPs dissolved in cyclohexane were mixed with ethanol and centrifuged at 12 000 rpm for 10 min. Then, the pellet was redispersed with a mixture of ethanol and an HCl aqueous solution (2 M) by sonication. The acid-treated UCNPs were thereafter washed three times with ethanol to remove excess acid. Subsequently, the ligand-free UCNPs were dispersed into deionized water for surface modification.

Poly(acrylic acid sodium salt) (PAA) was adopted for the surface modification of UCNPs. Ligand-free UCNPs were dropwise added to a poly(acrylic acid sodium salt) solution (10 mg mL^{-1}) while stirring. The solution was stirred overnight and thereafter purified three times with deionized water. PAA-coated UCNPs were dispersed in deionized water for further use.

Construction of UCNP nanoprobes

UCNP nanoprobes were constructed through the connection between UCNPs and *E. coli* aptamers. First, PAA-functionalized UCNPs were activated *via* EDC/Sulfo-NHS chemistry prior to the connection of aptamers. Next, amino-modified aptamers were added to the solution and stirred at 37 °C for 240 min. After that, 100 μL of mPEG-NH_2 (200 mg mL^{-1}) was reacted with UCNP-aptamer to reduce nonspecific binding effects. The successful construction of UCNP nanoprobes was characterized by fluorescence intensity and zeta potential.

Construction and optimization of the fluorescence biosensor

The biosensor was constructed by incubating the UCNP-Apt nanoprobes and GO@Fe_3O_4 in HEPES buffer (10 mM). The concentration of GO@Fe_3O_4 and the incubation time of UCNP-Apt nanoprobes were optimized for better detection performance.

Preparation of bacterial strains

Luria–Bertani (LB) medium solution was prepared and consisted of 5.00 g of sodium chloride, 2.50 g of yeast extract, 7.50 g of agarose G-10, 5.00 g of tryptone and 500 mL of ddH_2O. All bacterial strains were incubated with LB plates in an incubator containing 5% CO_2 at 37 °C for 16–24 h. McFarland turbidimetry was applied to quantify *E. coli*, *S. aureus*, *A. baumannii*, and *P. aeruginosa*. Bacterial suspensions with different concentrations (10^4, 10^5, 10^6, 10^7 and 10^8 CFU mL^{-1}) were prepared with PBS (0.01 mol L^{-1} and pH 7.4).

Evaluation of the analytical performance of the biosensor

For the *E. coli* assay, 50 μL of bacteria at different concentrations were incubated with the constructed biosensor for 30 min with gently shaking. After magnetic separation, the upconversion fluorescence intensity of the supernatant was measured. The number of bacteria was positively correlated with the intensity of the recovered fluorescence.

Specificity tests were completed by similar methods. *E. coli*, *S. aureus*, *A. baumannii*, *P. aeruginosa* and a mixed group containing the above bacteria at a final concentration of 10^7 CFU mL^{-1} were incubated with the prepared biosensor. The fluorescence intensity of the supernatant was measured for further comparison.

To evaluate the potential clinical application value of this biosensor, recovery tests were performed to detect bacteria in urine samples. All samples were kindly provided by the First Affiliated Hospital of Chongqing Medical University. The study had been approved by the ethics committee of the First Affiliated Hospital of Chongqing Medical University. And informed consent was obtained for all experiments on human subjects.

Results and discussion

Characterization of the UCNPs

The morphology and size of UCNPs were characterized by TEM. UCNP-PAA showed good dispersibility and a regular morphology in aqueous solution with a mean size of approximately 200 nm (Fig. 1A and B). Subsequently, the emission spectra of UCNPs were recorded with excitation at 980 nm. We observed that the nanomaterials had independent characteristic emission peaks at 475 nm (Fig. 2A, black line), which was attributed to the rare earth element Tm (Fig. 1C).

Fig. 1D shows the FTIR spectra. The bands at 2925 and 2854 cm^{-1} were assigned to the methylene (–CH_2–) asymmetric and symmetric stretching vibrations of OA in the alkyl chain. And the bands centred at 1563 and 1460 cm^{-1} were caused by the asymmetric and symmetric stretching vibrations of –COO– on the surface of the OA-coated UCNPs. After PAA modification,

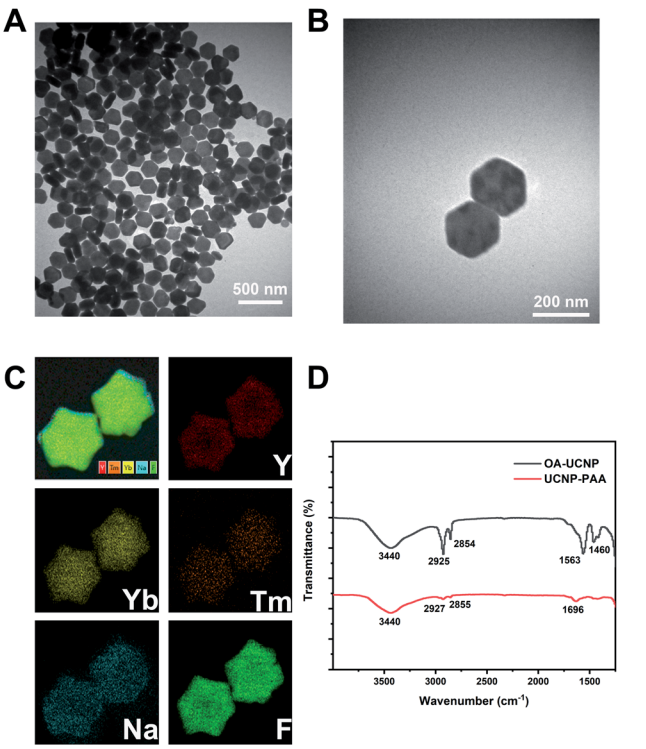

Fig. 1 Characterization of UCNPs: (A and B) TEM images of PAA-UCNPs, (C) elemental mappings of the UCNPs, and (D) FTIR spectra of OA-UCNP and UCNP-PAA.

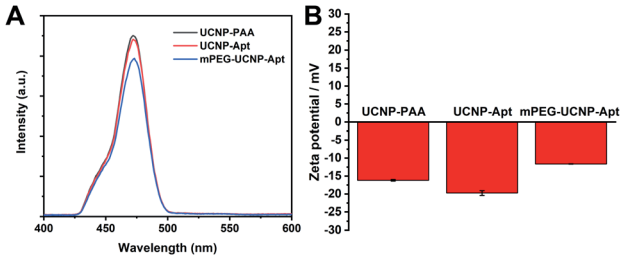

Fig. 2 Characterization of the construction process of UCNP-Apt nanoprobes: (A) fluorescence emission spectra of UCNP-PAA, UCNP-Apt and mPEG-UCNP-Apt and (B) zeta potentials of UCNP-PAA, UCNP-Apt and mPEG-UCNP-Apt.

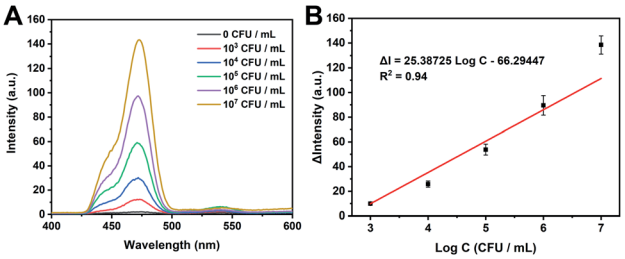

Fig. 4 Quantitative detection of *E. coli*. (A) Changes in the UCF signal of the biosensor after incubation with various concentrations of *E. coli*. (B) Linear relationship of the UCF intensity and the concentrations of *E. coli* from 10^3 to 10^7 CFU mL^{-1}. Error bars = SD ($n = 3$).

the bands attributed to the asymmetrical stretching of $-CH_2-$ groups at 2927 and 2855 cm^{-1} were reduced. Moreover, the bands at approximately 1696 cm^{-1} indicated an increased quantity of –COOH groups on the particle surface. These results demonstrated the successful PAA modification.

Characterization of the UCNP nanoprobes

Aptamers were connected to UCNP-PAA through amino-carboxyl chemistry to form UCNP-Apt nanoprobes. As seen in Fig. 2A, there was no significant change in UCNP fluorescence before and after aptamer functionalization. And after incubating with mPEG-NH_2, the fluorescence intensity was only slightly reduced, showing the excellent fluorescence stability of UCNPs. The zeta potential results indicated that the UCNPs and aptamers were connected successfully (Fig. 2B). The aptamers were negatively charged in the dispersion, after connecting to UCNP-PAA, the potential value was decreased from −16.18 mV to −19.73 mV. It indicated that the *E. coli* aptamers were connected onto the surface of UCNP-PAA successfully. mPEG-NH_2 was positively charged in the solution, after incubating with UCNP-Apt nanoprobes, and the potential value of UCNP-Apt nanoprobes was increased to −11.63 mV (Fig. 2B). It indicated that mPEG-NH_2 was modified successfully.

Construction and optimization of the biosensor

$GO@Fe_3O_4$ is another important part of this biosensor. The ultraviolet visible absorbance of $GO@Fe_3O_4$ was measured, and good fluorescence quenching ability was observed (Fig. S1†). Next, HEX-labelled aptamers were incubated with $GO@Fe_3O_4$ for 30 min and the fluorescence results showed that $GO@Fe_3O_4$ had the ability to bind single-stranded nucleic acids (Fig. S2†).

Subsequently, $GO@Fe_3O_4$ was added to UCNP nanoprobes to obtain final concentrations of 0.1 mg mL^{-1}, 0.2 mg mL^{-1}, 0.3 mg mL^{-1}, 0.4 mg mL^{-1}, 0.6 mg mL^{-1} and 0.8 mg mL^{-1}. As reflected in Fig. 3A, the quenching efficiency (see the ESI†) of $GO@Fe_3O_4$ increased with its concentration. However, when the concentration of $GO@Fe_3O_4$ was up to 0.4 mg mL^{-1}, the quenching efficiency increased to 90%, and there was no significant change with increasing concentration of $GO@Fe_3O_4$. To ensure that these nanoprobes were fully reacted, 0.6 mg mL^{-1} was selected as the optimized concentration of $GO@Fe_3O_4$.

Regarding the incubation time, 0.6 mg mL^{-1} $GO@Fe_3O_4$ was reacted with the UCNP nanoprobes for different periods of time. After 30 min of incubation, the quenching efficiency increased to 95%, and there was no significant change when the incubation time continued to increase (Fig. 3B). Therefore, 30 min was selected as the final incubation time.

Evaluation of analytical performance

Linear range and limit of detection. Regarding bacterial detection, different concentrations of bacteria were incubated with the constructed biosensor for 30 min with gentle shaking. The emission peaks of the upconversion luminescence for *E.*

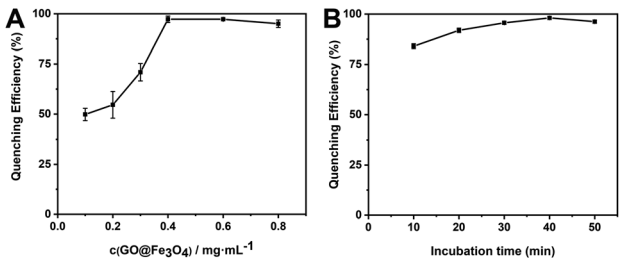

Fig. 3 Quenching efficiency of different concentrations of $GO@Fe_3O_4$ after incubation with the UCNP-Apt nanoprobes: (A) quenching efficiency of $GO@Fe_3O_4$ at different concentrations and (B) quenching efficiency of $GO@Fe_3O_4$ at different incubation times.

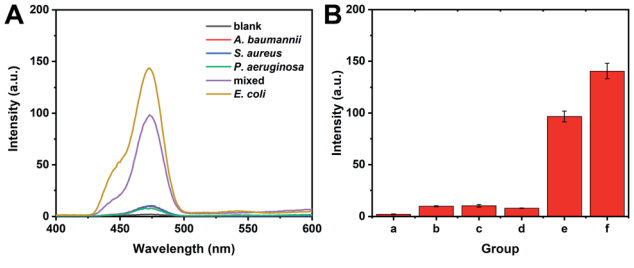

Fig. 5 Specificity of the biosensor for the detection of different bacteria: (A) fluorescence spectrum of different bacteria and, (B) fluorescence intensity of different bacteria at 475 nm: (a) blank control, (b) *A. baumannii*, (c) *S. aureus*, (d) *P. aeruginosa*, (e) mixed, and (f) *E. coli*. Error bars = SD ($n = 3$).

Table 1 Recovery tests of the fluorescence biosensor for *E. coli* detection

Sample no.	Spiked *E. coli* (log *C*)	Detected *E. coli* (log *C*)	Recovery (%)	RSD (%, $n = 10$)
1	3	3.05	101.7	0.63
2	5	4.78	95.6	3.35

coli were monitored at a wavelength of 475 nm. As shown in Fig. 4A, the change in fluorescence intensity ($\Delta\text{Intensity} = F - F_0$, F_0 was the fluorescence intensity measured in the control group) at 475 nm increased with increasing concentration of *E. coli*. It had a good linear relationship with the logarithm of *E. coli* concentrations ranging from 10^3 to 10^7 CFU mL^{-1} (Fig. 4B). This result indicated that *E. coli* could be quantified using the linear regression equation $\Delta\text{Intensity} = 25.38725 \log C - 66.29447$ with a linear correlation coefficient (R^2) of 0.94. The limit of detection (LOD) was estimated to be 467 CFU mL^{-1}. The published analytical methods for *E. coli* in the past three years have been collected for comparison (Table S1†). Compared with these analytical methods, this biosensor displays a good performance with respect to the analytical range and detection time.

Specificity. Specificity is another important indicator for assessing analytical methods. As illustrated in Fig. 5, there was no significant difference in the fluorescent signal between nontarget bacteria and the blank control. The luminescence signals were increased only in the presence of *E. coli*. This result indicated that the biosensor had good specificity towards *E. coli* and may be caused by the highly specific recognition ability between the aptamer and target bacteria.

Recovery tests. To further explore the potential application of this biosensor, pretreated urine samples were spiked with different concentrations of *E. coli*. The recovery rates were calculated to be 101.7% and 95.6% for *E. coli* at the concentrations of 10^3 and 10^5 CFU mL^{-1}, respectively (Table 1). These performances indicated that this detection method has high potential for clinical applications.

Conclusions

In summary, a fluorescent biosensor based on a FRET system was successfully constructed for the rapid detection of *E. coli*. These synthesized UCNPs had the ability to avoid autofluorescence originating from complex biological samples when excited with a 980 nm laser. As a fluorescence quencher, GO@Fe_3O_4 nanocomposites had many binding sites allowing a high loading of nanoprobes. The constructed biosensor could complete the whole detection process in 30 min with a linear range from 10^3 to 10^7 CFU mL^{-1} and the limit of detection was found to be 467 CFU mL^{-1}. Moreover, the biosensor was able to detect other bacteria through the use of certain aptamers. However, there were also some shortcomings that require improvement; for instance, the limit of detection needs to be further optimized. In summary, this biosensor has the opportunity to play a more important role in point-of-care testing with certain improvements in the future.

Author contributions

Yuan Yao: investigation, data curation, formal analysis, methodology, visualization, and writing – original draft. Guoming Xie: supervision, validation, visualization, and writing – review and editing. Xin Zhang: investigation, data curation, supervision, and methodology. Jinshan Yuan: methodology, supervision, and validation. Yulei Hou: data curation, supervision, and validation. Hui Chen: funding acquisition, project administration, resources, supervision, validation, and writing – review and editing.

Conflicts of interest

There are no conflicts to declare.

Acknowledgements

This research work was financially supported by the Chongqing Science and Technology Bureau (No. cstc2019jscx-msxmX0088), the National Natural Science Foundation of China (No. 81972011) and the Chongqing Municipal Health Commission (No. 2020MSXM009).

Notes and references

1 R. D. Klein and S. J. Hultgren, *Nat. Rev. Microbiol.*, 2020, **18**, 211–226.
2 S. Lee, V. S. L. Khoo, C. A. D. Medriano, T. Lee, S. Y. Park and S. Bae, *Water Res.*, 2019, **160**, 371–379.
3 A. C. Vinayaka, T. A. Ngo, K. Kant, P. Engelsmann, V. P. Dave, M. A. Shahbazi, A. Wolff and D. D. Bang, *Biosens. Bioelectron.*, 2019, **129**, 224–230.
4 S. Han, M. C. Soylu, C. E. Kirimli, W. Wu, B. Sen, S. G. Joshi, C. L. Emery, G. Au, X. Niu, R. Hamilton, K. Krevolin, W. H. Shih and W. Y. Shih, *Biosens. Bioelectron.*, 2019, **130**, 73–80.
5 J. D. Perry, *Clin. Microbiol. Rev.*, 2017, **30**, 449–479.
6 F. Roux-Dalvai, C. Gotti, M. Leclercq, M. C. Helie, M. Boissinot, T. N. Arrey, C. Dauly, F. Fournier, I. Kelly, J. Marcoux, J. Bestman-Smith, M. G. Bergeron and A. Droit, *Mol. Cell. Proteomics*, 2019, **18**, 2492–2505.
7 E. A. Idelevich, K. Sparbier, M. Kostrzewa and K. Becker, *Clin. Microbiol. Infect.*, 2018, **24**, 738–743.
8 M. Kallsten, M. Pijnappel, R. Hartmann, F. Lehmann, L. Kovac, S. B. Lind and J. Bergquist, *Anal. Bioanal. Chem.*, 2019, **411**, 2569–2576.
9 V. Vedarethinam, L. Huang, W. Xu, R. Zhang, D. D. Gurav, X. Sun, J. Yang, R. Chen and K. Qian, *Small*, 2019, **15**, e1803051.
10 T. H. Liu, S. S. Cheng, H. L. You, M. S. Lee and G. B. Lee, *Analyst*, 2019, **144**, 1210–1222.

11 S. Sharifi, S. Z. Vahed, E. Ahmadian, S. M. Dizaj, A. Eftekhari, R. Khalilov, M. Ahmadi, E. Hamidi-Asl and M. Labib, *Biosens. Bioelectron.*, 2020, **150**, 111933.
12 F. Schaumburg, C. S. Carrell and C. S. Henry, *Anal. Chem.*, 2019, **91**, 9623–9630.
13 S. Singh, A. Moudgil, N. Mishra, S. Das and P. Mishra, *Biosens. Bioelectron.*, 2019, **136**, 23–30.
14 X. Zhang, G. Xie, D. Gou, P. Luo, Y. Yao and H. Chen, *Biosens. Bioelectron.*, 2019, **142**, 111486.
15 M. Yu, H. Wang, F. Fu, L. Li, J. Li, G. Li, Y. Song, M. T. Swihart and E. Song, *Anal. Chem.*, 2017, **89**, 4085–4090.
16 Y. Si, C. Grazon, G. Clavier, J. Rieger, J.-F. Audibert, B. Sclavi and R. Méallet-Renault, *Biosens. Bioelectron.*, 2016, **75**, 320–327.
17 P. Lavaee, S. M. Taghdisi, K. Abnous, N. M. Danesh, L. H. Khayyat and S. H. Jalalian, *Talanta*, 2019, **202**, 349–353.
18 M. Toma, S. Izumi and K. Tawa, *Analyst*, 2018, **143**, 858–864.
19 L. Zhang, J. Peng, M. F. Hong, J. Q. Chen, R. P. Liang and J. D. Qiu, *Mikrochim. Acta*, 2019, **186**, 309.
20 Q. Li, X. Liang, X. Mu, L. Tan, J. Lu, K. Hu, S. Zhao and J. Tian, *Mikrochim. Acta*, 2020, **187**, 365.
21 L. K. Muller, I. Duznovic, D. Tietze, W. Weber, M. Ali, V. Stein, W. Ensinger and A. A. Tietze, *Chemistry*, 2020, **26**, 8511–8517.
22 M. Wei, F. Zhao and Y. Xie, *Talanta*, 2020, **209**, 120599.
23 B. Zhou, B. Shi, D. Jin and X. Liu, *Nat. Nanotechnol.*, 2015, **10**, 924–936.
24 J. Zhao, J. Gao, W. Xue, Z. Di, H. Xing, Y. Lu and L. Li, *J. Am. Chem. Soc.*, 2018, **140**, 578–581.
25 H. Xin, Y. Li, D. Xu, Y. Zhang, C. H. Chen and B. Li, *Small*, 2017, **13**(14), 1603418.
26 W. Li, K. Dong, H. Wang, P. Zhang, Y. Sang, J. Ren and X. Qu, *Biomaterials*, 2019, **217**, 119310.
27 K. Zhang, S. Song, S. Huang, L. Yang, Q. Min, X. Wu, F. Lu and J. J. Zhu, *Small*, 2018, **14**, e1802292.
28 R. Chand, N. Mittal, S. Srinivasan and A. R. Rajabzadeh, *Analyst*, 2021, **146**, 574–580.
29 L. Liu, H. Zhang, D. Song and Z. Wang, *Analyst*, 2018, **143**, 761–767.
30 H. Rabie, Y. Zhang, N. Pasquale, M. J. Lagos, P. E. Batson and K. B. Lee, *Adv. Mater.*, 2019, **31**, e1806991.
31 R. Peltomaa, Z. Farka, M. J. Mickert, J. C. Brandmeier, M. Pastucha, A. Hlavacek, M. Martinez-Orts, A. Canales, P. Skladal, E. Benito-Pena, M. C. Moreno-Bondi and H. H. Gorris, *Biosens. Bioelectron.*, 2020, **170**, 112683.
32 L. Yang, K. Zhang, S. Bi and J. J. Zhu, *ACS Appl. Mater. Interfaces*, 2019, **11**, 38459–38466.
33 N. Parvin, Q. Jin, Y. Wei, R. Yu, B. Zheng, L. Huang, Y. Zhang, L. Wang, H. Zhang, M. Gao, H. Zhao, W. Hu, Y. Li and D. Wang, *Adv. Mater.*, 2017, **29**(18), 1606755.
34 Q. Li, Y. Wang, G. Yu, Y. Liu, K. Tang, C. Ding, H. Chen and S. Yu, *Nanoscale*, 2019, **11**, 20903–20909.
35 F. S. Awad, K. M. AbouZied, A. M. Bakry, W. M. Abou El-Maaty, A. M. El-Wakil and M. S. El-Shall, *Anal. Chim. Acta*, 2020, **1140**, 111–121.
36 X. Ou, S. Zhan, C. Sun, Y. Cheng, X. Wang, B. Liu, T. Zhai, X. Lou and F. Xia, *Biosens. Bioelectron.*, 2019, **124–125**, 199–204.
37 Y. Zhang, X. Chen, G. M. Roozbahani and X. Guan, *Analyst*, 2019, **144**, 1825–1830.
38 D. Gou, G. Xie, Y. Li, X. Zhang and H. Chen, *Mikrochim. Acta*, 2018, **185**, 436.
39 J. Ke, S. Lu, X. Shang, Y. Liu, H. Guo, W. You, X. Li, J. Xu, R. Li, Z. Chen and X. Chen, *Adv. Sci.*, 2019, **6**, 1901874.

